Advances in Applied Mathematics and Mechanics
Adv. Appl. Math. Mech., Vol. **10**, No. 6, pp. 1459-1477

DOI: 10.4208/aamm.OA-2018-0103
December 2018

A Regularized Singular Boundary Method for Inverse Cauchy Problem in Three-Dimensional Elastostatics

Aixia Zhang[1], Yan Gu[1,*], Qingsong Hua[2], Wen Chen[3] and Chuanzeng Zhang[4]

[1] *School of Mathematics and Statistics, Qingdao University, Qingdao 266071, Shandong, China*
[2] *School of Mechanical Engineering, Qingdao University, Qingdao 266071, Shandong, China*
[3] *Department of Engineering Mechanics, College of Mechanics and Materials, Hohai University, Nanjing 210098, Jiangsu, China*
[4] *Department of Civil Engineering, University of Siegen, Paul-Bonatz-Str. 9-11, D-57076 Siegen, Germany*

Received 16 April 2018; Accepted (in revised version) 13 June 2018

Abstract. The application of the singular boundary method (SBM), a relatively new meshless boundary collocation method, to the inverse Cauchy problem in three-dimensional (3D) linear elasticity is investigated. The SBM involves a coupling between the non-singular boundary element method (BEM) and the method of fundamental solutions (MFS). The main idea is to fully inherit the dimensionality advantages of the BEM and the meshless and integration-free attributes of the MFS. Due to the boundary-only discretizations and its semi-analytical nature, the method can be viewed as an ideal candidate for the solution of inverse problems. The resulting ill-conditioned algebraic equations is regularized here by employing the first-order Tikhonov regularization technique, while the optimal regularization parameter is determined by the *L*-curve criterion. Numerical results with both smooth and piecewise smooth geometries show that accurate and stable solution can be obtained with a comparatively large level of noise added into the input data.

AMS subject classifications: 62P30, 65M32, 65K05

Key words: Meshless method, singular boundary method, method of fundamental solutions, elastostatics, inverse problem.

1 Introduction

*Corresponding author.
Email: guyan1913@163.com (Y. Gu)

 ©2018 Global Science Press

Over the past two decades, some considerable effort was devoted to proposing novel computational algorithms that circumvent or greatly eliminate the problems associated with the domain and/or boundary meshing. This led to the development of various meshless or meshfree methods [1–4]. These methods, generally, can be divided into the domain-type or boundary-type schemes, depending on whether their basis functions satisfy the governing equation of interest [5–8]. For an overview of the state of the art, we refer interested readers to articles [9–14] for existing theoretical results, different algorithms, and software packages.

The singular boundary method (SBM) [15–21] is a relatively new boundary-type meshless method for the numerical solution of boundary value problems governed by certain partial differential equations. The method involves a coupling between the non-singular boundary element method (BEM) [22,23] and the method of fundamental solutions (MFS) [7,9,24–29]. The key idea of the method is to fully inherit the dimensionality and stability advantages of the BEM and the meshless and integration-free attributes of the MFS. The method keeps the advantage of simplicity of the MFS and meanwhile sidesteps the troublesome fictitious boundary issue associated with the later. The key idea of the SBM was proposed in the early 2000s by Chen and Wang [30] and were later essentially improved and extended by many other authors [31–33]. Prior to this study, this method has been successfully tried for two-dimensional (2D) problems in potential and elasticity theories [15], acoustic radiation and scattering problems [18], inverse heat conduction problems [34], thin-walled structural problems [35], as well as large-scale modelling for 3D heat conduction problems [36].

Motivated by the rapidly growing interest in the area, this paper documents the first attempt to extend the SBM for the solution of inverse Cauchy problems arising in 3D elastostatics. In inverse problems, one or more of the data describing the direct problem is missing. To fully determine the process, additional data must be supplied, either other boundary conditions on the same accessible part of boundary or measurements at some internal points in the domain [37]. The inverse problems are, generally, difficult to solve numerically due to the fact that they are ill-posed in the sense that small errors in measured data may lead arbitrarily large changes in the numerical solution [38–40]. The resulting ill-conditioned algebraic equations are regularized here by employing the first-order Tikhonov regularization technique [7], while the optimal regularization parameter is determined by the L-curve criterion [41]. It is shown that the SBM can be viewed as an ideal candidate for the solution of inverse Cauchy problems, due to the boundary-only discretizations and its semi-analytical nature.

A brief outline of the rest of the paper is as follows. In Section 2, the mathematical formulation for 3D elasticity problems is briefly introduced. The methodology of the SBM and its numerical implementation for 3D elastostatics are reviewed in Section 3. The Tikhonov regularization method with the choice of the regularization parameter given by the L-curve criterion is presented in Section 4. Next in Section 5, three benchmark numerical examples involving both smooth and piecewise smooth geometries are investigated. Finally, some conclusions and remarks are provided in Section 6.

2 Statement of the basic problem

In the absence of body forces, the equilibrium equations for 3D problems in linear elasticity, in terms of the displacements $u_i(x)$, $i=1,2,3$, can be stated as [42]

$$c_1\frac{\partial^2 u_1(x)}{\partial x_1^2}+\frac{\partial^2 u_1(x)}{\partial x_2^2}+\frac{\partial^2 u_1(x)}{\partial x_3^2}+c_2\frac{\partial^2 u_2(x)}{\partial x_1\partial x_2}+c_2\frac{\partial^2 u_3(x)}{\partial x_1\partial x_3}=0, \tag{2.1a}$$

$$c_2\frac{\partial^2 u_1(x)}{\partial x_1\partial x_2}+\frac{\partial^2 u_2(x)}{\partial x_1^2}+c_1\frac{\partial^2 u_2(x)}{\partial x_2^2}+\frac{\partial^2 u_2(x)}{\partial x_3^2}+c_2\frac{\partial^2 u_3(x)}{\partial x_2\partial x_3}=0, \tag{2.1b}$$

$$c_2\frac{\partial^2 u_1(x)}{\partial x_1\partial x_3}+c_2\frac{\partial^2 u_2(x)}{\partial x_2\partial x_3}+\frac{\partial^2 u_3(x)}{\partial x_1^2}+\frac{\partial^2 u_3(x)}{\partial x_2^2}+c_1\frac{\partial^2 u_3(x)}{\partial x_3^2}=0, \tag{2.1c}$$

subject to the boundary conditions

$$u_i(x)=\bar{u}_i(x), \qquad x\in\Gamma_u \quad \text{(Dirichlet boundary conditions)}, \tag{2.2a}$$

$$t_i(x)=\sigma_{ij}(x)n_j(x)=\bar{t}_i(x), \qquad x\in\Gamma_t \quad \text{(Neumann boundary conditions)}, \tag{2.2b}$$

where $c_1=\frac{2-2\nu}{1-2\nu}$, $c_2=\frac{1}{1-2\nu}$, ν denotes Poisson's ratio, $t_i(x)$ are boundary tractions, $n_j(x)$ are the outward unit normal vector, Γ_u and Γ_t comprise the whole boundary of the computational domain, $\sigma_{ij}(x)$ denote stresses, the barred quantities $\bar{u}_i$ and $\bar{t}_i$ indicate the given displacement and traction values specified on the boundary. Here and in the following, the customary Einstein's notation for summation over repeated subscripts is applied.

The kinematics of deformation is described by the linear strain tensor

$$\varepsilon_{ij}(x)=\frac{1}{2}\left\{\frac{\partial u_i(x)}{\partial x_j}+\frac{\partial u_j(x)}{\partial x_i}\right\}, \tag{2.3}$$

where sufficiently small displacements and displacement gradients are assumed. The stresses $\sigma_{ij}(x)$ are related to the strains $\varepsilon_{ij}(x)$ through Hooke's law by

$$\sigma_{ij}(x)=2G\left(\varepsilon_{ij}(x)+\frac{\nu}{1-2\nu}\varepsilon_{kk}(x)\delta_{ij}\right), \tag{2.4}$$

where G stands for the shear modulus, δ_{ij} is the well-known Kronecker delta. The boundary tractions t_i are then defined in terms of the stresses as follows

$$t_i(x)=\sigma_{ij}(x)n_j(x). \tag{2.5}$$

Employing indicial notation for the coordinates of points x and y, i.e., $x=(x_1,x_2,x_3)$ and $y=(y_1,y_2,y_3)$, respectively, the Kelvin fundamental solutions for 3D elasticity problems can be expressed as follows (see, e.g., [5, 42])

$$U_{ij}(y,x)=\frac{1}{16\pi G(1-\nu)r}\left[(3-4\nu)\delta_{ij}+r_{,i}r_{,j}\right], \quad i,j=1,2,3, \tag{2.6}$$

where

$$r=\sqrt{(x_1-y_1)^2+(x_2-y_2)^2+(x_3-y_3)^2}$$

denotes the Euclidean distance between points x and y, the comma denotes partial differentiation with respect to the spatial coordinates, e.g., $r_{,i}=(y_i-x_i)/r$. On taking into account the kinematic relations (2.3), the Hooke's law (2.4), and the definitions of the components of the traction vector (2.5), the fundamental solutions for stresses $D_{ijk}(y,x)$ and tractions $T_{ij}(y,x)$ can be expressed as

$$D_{ijk}(y,x)=\frac{1}{8\pi(1-\nu)r^2}\left[(1-2\nu)\left(r_{,k}\delta_{ij}-r_{,i}\delta_{jk}-r_{,j}\delta_{ik}\right)-3r_{,i}r_{,j}r_{,k}\right], \tag{2.7a}$$

$$\begin{aligned}T_{ij}(y,x)=-\frac{1}{8\pi(1-\nu)r^2}\Big[&(1-2\nu)(r_{,i}n_j(y)-r_{,j}n_i(y))\\&+r_{,k}n_k(y)((1-2\nu)\delta_{ij}+3r_{,i}r_{,j})\Big].\end{aligned} \tag{2.7b}$$

In the direct problem formulation, the knowledge of the displacements and tractions are prescribed on boundaries Γ_u and Γ_t, respectively. If it is possible to measure both displacements and tractions on a part of the boundary, say Γ_1, then this leads to the mathematical formulation of an inverse Cauchy problem consisting of equations (2.1a)-(2.1c) and the following boundary conditions

$$u_i(x)=\bar{u}_i(x),\quad t_i(x)=\bar{t}_i(x),\quad x\in\Gamma_1. \tag{2.8}$$

In the above formulation, it can be seen that the boundary Γ_1 is over-specified, whilst the remaining boundary, say Γ_2, is under-specified since both the displacements and tractions are unknown and have to be determined.

3 Singular boundary method: mathematical background and numerical implementation

Similar to the MFS, the SBM also uses the fundamental solution as the basis function of its interpolation. In contrast to the MFS, the SBM sidesteps the perplexing fictitious boundary issue associated with the MFS by means of the introduction of origin intensity factors, a numerical strategy that isolate the singularities of the fundamental solutions and allows the coincidence of the source and collocation points.

The SBM interpolation for 3D elasticity problems can be expressed as [5]

$$u_i(y^m)=\sum_{\substack{n=1\\n\neq m}}^{N}\alpha_j^n U_{ij}(y^m,x^n)+\alpha_j^m A_{ij},\qquad y^m\in\Gamma_u, \tag{3.1a}$$

$$t_i(y^m)=\sum_{\substack{n=1\\n\neq m}}^{N}\alpha_j^n T_{ij}(y^m,x^n)+\alpha_j^m B_{ij},\qquad y^m\in\Gamma_t, \tag{3.1b}$$

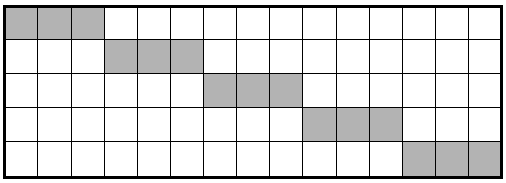

Figure 1: The SBM interpolation matrix for 3D elasticity problems (the shadow areas indicate the origin intensity factors).

where $i,j=1,2,3$, $\{\alpha_j^n\}_{n=1}^N$ represent the unknown coefficients to be calculated, $y^m \in \bar{\Omega} = \Omega \bigcup \partial\Omega$ is the mth collocation (calculation) point, x^n stands for the n-th source point, which lies along the real boundary of the computational domain. In Eqs. (3.1a) and (3.1b), A_{ij} and B_{ij} are defined as the origin intensity factors, i.e., the singular terms when point x coincides with point y (the shadow areas shown in Fig. 1).

Observe that when points x and y coincide with each other, the term A_{ij} have a weak singularity of order $(1/r)$ in 3D elastic problems, while B_{ij} present a strong singularity of order $(1/r^2)$. The key point in achieving the required accuracy and efficiency of the SBM is the accurate evaluation of such singular terms. Quite recently, Gu and his collaborators [5, 43] have provided efficient algorithms for the direct calculation of the above-mentioned origin intensity factors. The methods can be successfully applied to 2D and 3D SBM formulations, regardless of the specific class of problems being considered and whatever the type and order of the singular terms encountered. For completeness, the main results for 3D elastic problems are summarized hereafter.

We first recall the following indirect BEM formulation in the form of a single-layer potential to represent the displacement field

$$u_i(y) = \int_\Gamma a_j(x) U_{ij}(y,x) d\Gamma_x, \tag{3.2}$$

where $y \in \bar{\Omega} = \Omega \bigcup \partial\Omega$ and $a_j(x)$ denote unknown densities. According to singular-layer potential theory, the displacement field (3.2) is continuous throughout the domain as well as across the boundary. The surface tractions, however, undergo a discontinuity across the boundary [44],

$$t_i(\mathbf{y}) = c_{ij}(\mathbf{y}) a_j(\mathbf{y}) + \neg\!\!\!\!\int_\Gamma a_j(\mathbf{x}) T_{ij}(\mathbf{y},\mathbf{x}) d\Gamma_{\mathbf{x}}, \quad \mathbf{y} \to \Gamma, \tag{3.3}$$

where $c_{ij}(\mathbf{y})$ are the coefficients of the free terms, and $c_{ij} = \delta_{ij}/2$ for a smooth boundary. The symbol $\neg\!\!\!\!\int$ denotes the integration in the Cauchy principal value (CPV) sense [5].

Let Γ_m be the element containing the singular point $\mathbf{y}$, then Eqs. (3.2) and (3.3) can be split into, at the singular element Γ_m, as follows

$$u_i(y) = \int_{\Gamma - \Gamma_m} a_j(x) U_{ij}(y,x) d\Gamma_x + \int_{\Gamma_m} a_j(x) U_{ij}(y,x) d\Gamma_x, \tag{3.4a}$$

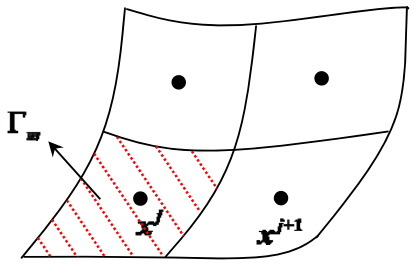

Figure 2: Nodal integration domain for three-dimensional problems.

$$t_i(\mathbf{y}) = \frac{1}{2}a_i(\mathbf{y}) + \int_{\Gamma-\Gamma_m} a_j(\mathbf{x})T_{ij}(\mathbf{y},\mathbf{x})d\Gamma_{\mathbf{x}} + \oint_{\Gamma_m} a_j(\mathbf{x})T_{ij}(\mathbf{y},\mathbf{x})d\Gamma_{\mathbf{x}}. \tag{3.4b}$$

Considering a discretized approach of the above integral equations one gets

$$u_i(y^m) \approx \sum_{\substack{n=1 \\ n\neq m}}^{N} \alpha_j^n U_{ij}(y^m,x^n) + \alpha_j^m \langle U_{ij}(y^m,x)\rangle, \tag{3.5a}$$

$$t_i(\mathbf{y}^m) \approx \frac{1}{2}\frac{\alpha_i^m}{L_m} + \sum_{\substack{n=1 \\ n\neq m}}^{N} \alpha_j^n T_{ij}(\mathbf{y}^m,\mathbf{x}^n) + \alpha_j^m \langle T_{ij}(\mathbf{y}^m,\mathbf{x})\rangle, \tag{3.5b}$$

where $\mathbf{y}^m \in \partial\Omega$ is the mth collocation point, L_m denotes the area of Γ_m (see Fig. 2), $\langle\cdot\rangle$ means the averaged value of the fundamental solutions over Γ_m, i.e.,

$$\langle U_{ij}(y^m,x)\rangle = \frac{1}{L_m}\int_{\Gamma_m} U_{ij}(y^m,x)d\Gamma_x, \tag{3.6a}$$

$$\langle T_{ij}(y^m,x)\rangle = \frac{1}{L_m}\Gamma_m T_{ij}(y^m,x)d\Gamma_x, \tag{3.6b}$$

where, as mentioned above, the kernels $U_{ij}(y,x)$ present a weak singularity of order $(1/r)$, while $T_{ij}(\mathbf{y},\mathbf{x})$ have a strong singularity of order $(1/r^2)$.

Algorithms related to the direct evaluation of weakly singular integrals (3.6a) are widely available, see for example, [45, 46]. An accurate approximation to the singular term (3.6b) is given by Gu et al. in [5],

$$\begin{aligned}&\langle T_{ij}(y^m,x)\rangle \\ &= \int_0^{2\pi}\int_0^{\beta(\theta)} \left[F_{ij}(\rho,\theta) - \frac{f_{ij}(\theta)J(\eta)}{\rho}\right]d\rho d\theta + \int_0^{2\pi} f_{ij}(\theta)J(\eta)\ln[\beta(\theta)A(\theta)]d\theta,\end{aligned} \tag{3.7}$$

where ρ and θ denote the local polar coordinate system, $F_{ij}(\rho,\theta)$ and $f_{ij}(\theta)$ are functions which consist of the fundamental solutions and the Jacobian of the transformation from the boundary surface to local polar coordinate system. Details on the derivations of some

of these formulas can be found in [5]. The numerical evaluation of the regular integral in (3.7) can be easily accomplished by using the standard Gaussian quadrature formulae. In order to make the SBM integration-free, we use the well-known Trapezoidal quadrature formula in our computations.

Using the procedure described above, the following SBM formulation for boundary tractions can be obtained

$$t_i(\mathbf{y}^m) = \sum_{\substack{n=1 \\ n\neq m}}^{N} \alpha_j^n T_{ij}(\mathbf{y}^m, \mathbf{x}^n) + \alpha_j^m B_{ij}^m, \tag{3.8}$$

where

$$B_{ij}^m = \frac{1}{L_m}\left(\frac{\delta_{ij}}{2} + \langle T_{ij}(y^m, x)\rangle\right) \tag{3.9}$$

is defined as the origin intensity factors for Neumann boundary conditions. Now, we can develop a slight modification of the traditional MFS for 3D elasticity problems, which can be summarized in the following steps:

Step 1 Distributing a number of N source points over the boundary.

Step 2 When point $\mathbf{x}$ is far away from point y, the corresponding terms of the coefficient matrix are computed directly in a way similar to the MFS.

Step 3 When point $\mathbf{x}$ coincides with point y, set the singular term as the averaged value of the fundamental solution over an auxiliary boundary which is defined by the semi-length distance of the source points, see Eqs. (3.5a) and (3.5b).

For a well-posed boundary value problem, the unknown coefficients $\{\alpha_j^n\}_{n=1}^N$ can be calculated by collocating N observation points on the boundary conditions. In the inverse Cauchy problems, if the total number of M collocation points are discretized on the whole boundary in which the number of N points are chosen on the over-specified boundary Γ_1, then Eqs. (3.5a) and (3.5b) generate a system of $6N$ linear algebraic equations with $3M$ unknowns

$$\mathbf{A}\mathbf{x} = \mathbf{b}, \tag{3.10}$$

where $\mathbf{A}$, $\mathbf{x}$ and $\mathbf{b}$ denote the SBM matrix, the unknown vector and the right-hand side vector, respectively. The system of such linear algebraic equations, as illustrated in [7], cannot be solved accurately by using the conventional Gaussian elimination method or other methods designed for direct problems. Nevertheless, some regularization techniques should be employed for their evaluation, which will be briefly presented in the following section.

Once all coefficients $\{\alpha_j^n\}_{n=1}^N$ are computed, the displacements and stresses at any point inside the domain can be obtained using the following strong-form formula

$$u_i(y)=\sum_{n=1}^{N}\alpha_j^n U_{ij}(y,x^n), \tag{3.11a}$$

$$\sigma_{ij}(y)=\sum_{n=1}^{N}\alpha_k^n D_{ijk}(y,x^n), \tag{3.11b}$$

where U_{ij} and D_{ijk} are fundamental solutions for displacements and stresses, as shown in Eqs. (2.6) and (2.7a).

4 Regularization techniques for inverse problems

One widely used regularization technique for solving ill-conditioning problem is the Tikhonov regularization method, which considers a minimum of the following function

$$f_\lambda(x)=\|Ax-b\|_2^2+\lambda^2\left\|L^{(i)}x\right\|_2^2,\quad L^{(i)}\in R^{(N-i)\times N},\quad i=0,1,2,\cdots, \tag{4.1}$$

where λ is the regularization parameter, $\|\cdot\|_2$ denotes the Euclidean norm, $L^{(i)}$ is a matrix that defines a (semi) norm of solution vector in which the superscript (i) represents the i-th derivative operator on L, for example, in the case of the first-order Tikhonov regularization method the matrix $\mathbf{L}^{(i)}$ is given by

$$\mathbf{L}^{(1)}=\begin{bmatrix}-1 & 1 & 0 & \cdots & 0\\ 0 & -1 & 1 & \cdots & 0\\ \vdots & \vdots & \vdots & \ddots & \vdots\\ 0 & 0 & \cdots & -1 & 1\end{bmatrix}_{(N-1)\times N}. \tag{4.2}$$

Solving $\nabla f_\lambda(x)=0$ for $x\in R^N$, we can obtain the Tikhonov regularized solution x_λ of the Eq. (4.1), which is given as the solution of the regularized equation

$$(\mathbf{A}^T\mathbf{A}+\lambda^2\mathbf{L}^{(i)^T}\mathbf{L}^{(i)})\mathbf{x}=\mathbf{A}^T\mathbf{b}. \tag{4.3}$$

The performance of the Tikhonov method depends crucially on a suitable choice of the regularization parameter λ. The L-curve criterion is frequently used. The L-curve is a log-log plot of the norm of regularized solution ($\|L^{(i)}x\|_2$) versus the norm of the corresponding residual norm ($\|Ax-b\|_2$), i.e., as a curve

$$\left(\log\|Ax-b\|_2,\log\left\|L^{(i)}x\right\|_2\right), \tag{4.4}$$

parametrized by the regularization parameter. The horizontal part of the L-curve corresponds to the index of how smooth the solution is treated, and the vertical part of the

L-curve corresponds to the distance index between the predicted output and real output. The corner point of L-curve is a compromise between the regularization errors due to data smoothing and perturbation errors in measurements or other noise. Hence, the L-curve is really a trade-off curve between two quantities that both should be controlled and, according to the L-curve criterion, the optimal value of the regularization parameter is chosen at the "corner" of the L-curve, see [7].

5 Numerical results and discussions

In this section, three benchmark numerical examples associated with 3D elastic equations are presented to verify the methodologies developed above. The effect of regularization as well as the stability of the scheme with respect to the noise added into the data are carefully investigated. For the ease of comparison and validation of the numerical results, we considered the following analytical solutions

$$u_i(x)=x_1+x_2+x_3, \quad i=1,2,3, \tag{5.1}$$

for displacements, and

$$\sigma_{11}(x)=\sigma_{22}(x)=\sigma_{33}(x)=\frac{2G(1+\nu)}{1-2\nu}, \quad \sigma_{12}(x)=\sigma_{13}(x)=\sigma_{23}(x)=2G, \tag{5.2}$$

for stresses. The elasticity parameters are taken to be $\nu=0.2$ (Poisson's ratio) and $G=$ 13889 (shear modulus). In order to evaluate the performance of the numerical method, an L_2 error norm is defined as follows:

$$\text{Global Error}=\Big[\sum_{k=1}^{M}\Big[I_{\text{numer}}(k)-I_{\text{exact}}(k)\Big]^2\Big]^{1/2}\Big/\Big[\sum_{k=1}^{M}\Big[I_{\text{exact}}(k)\Big]^2\Big]^{1/2}, \tag{5.3}$$

where $I_{\text{numerical}}(k)$ and $I_{\text{exact}}(k)$ denote the numerical and analytical solutions at the kth calculated point, respectively, M is the number of calculation points tested. In our test cases, the simulated noisy data are generated using the following formula

$$\tilde{b}=b\Big(1+rand\times\frac{\delta}{100}\Big), \tag{5.4}$$

where b is the exact boundary data, $rand$ is a random number and its range is $-1\leq rand\leq$ 1, and δ stands for the level of noise. In our computations, the random variable rand was realized using the Matlab function "rand".

Unless otherwise specified, the measure of the accessible (or over-specified) boundary is defined as $\Gamma_1=BL\times\Gamma$ in which

$$BL=\frac{measure(\Gamma_1)}{measure(\Gamma)}, \quad BL\in(0,1], \tag{5.5}$$

denotes the ratio parameter of the accessible boundary.

5.1 Test problem 1: problem with a piecewise geometry

As a first example let us consider the solution of the Navier equations in a domain with a piecewise smooth geometry $\Omega=(-0.5,0.5)^3\backslash[-0.5,0]^3$, as shown in Fig. 3. To solve the problem numerically, $M=480$ evenly distributed source points are chosen on the boundary. In this example the upper surface $S_6=\{(x_1,x_2,x_3)|x_3=0.5\}$ and the right-hand side surface $S_1=\{(x_1,x_2,x_3)|x_2=0.5\}$ are under-specified where both the displacements and tractions are unknown and have to be determined.

Before presenting the numerical results obtained using regularization methods, it is interesting to investigate the necessity for employing such regularization technique when solving an ill-posed Cauchy problem. To do this, we illustrate the displacement results obtained on the under-specified surface $S_6=\{(x_1,x_2,x_3)|x_3=0.5\}$ using 2% noisy Cauchy data. We found that, similar to the results illustrated in [47], the displacement results are highly inaccurate and divergent, with the relative error is larger than 10^5. Thus, the SBM, without employing the regularization technique, could not yield accurate results for noisy data.

Figs. 4(a)-(d) illustrate the analytical (solid lines) and the numerical results (dashed lines) for the displacements u_1 obtained on the under-specified surface $S_6=\{(x_1,x_2,x_3)|x_3=0.5\}$, using various levels of noise added into the input data. It can be seen that the numerical results retrieved for displacements are in good agreement with their corresponding analytical solutions, even with a relatively large amount of noise (3%). It can be observed that, as expected, the numerical solutions converge to their corresponding analytical solutions as the amount of noise decreases. It can be conclude that the numerical solutions retrieved for this 3D case are stable and accurate. Although not presented here, it should be noted that analogous results have been obtained for the other components of the displacement vectors on both the two under-specified boundaries. The value of regularization parameter for 3% noise, as shown in Eq. (4.1), is $\lambda=0.018$.

Moreover, a similar conclusion can be drawn from Figs. 5(a)-(d) which present the numerical results retrieved for tractions t_1 on the under-specified surface $S_6=$

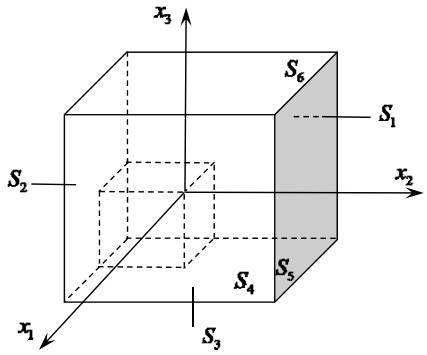

Figure 3: Solution of the Navier equations in a domain with a piecewise smooth geometry.

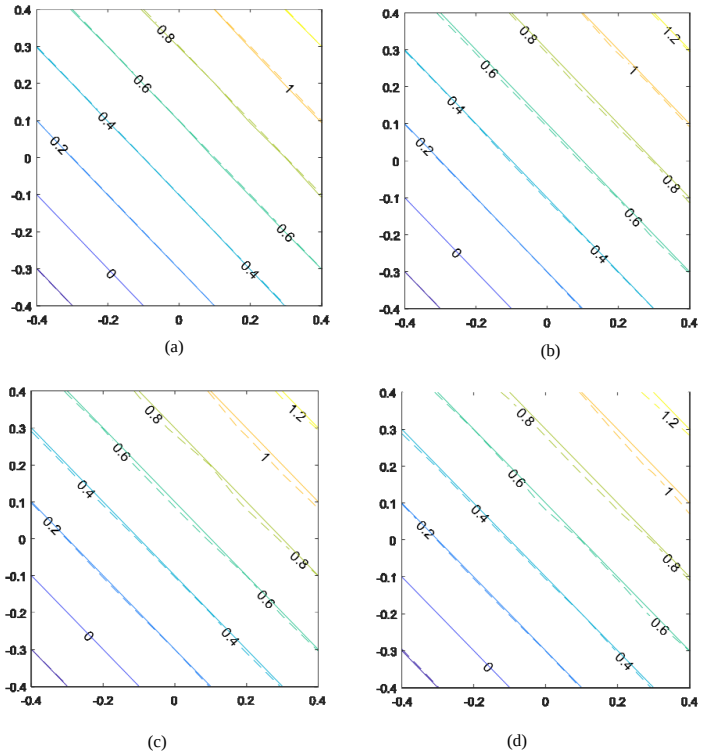

Figure 4: Numerical displacements u_1 retrieved on the under-specified boundary, with (a) 0% noisy, (b) 1% noisy, (c) 2% noisy, and (d) 3% noisy added into the input data.

$\{(x_1,x_2,x_3)|x_3=0.5\}$, using various levels of noise added into the input data. Similar results have been obtained for other components of traction vectors, as well as for stresses in the cases with other combinations of boundary conditions. Hence the SBM, in conjunction with the Tikhonov regularization technique, provides stable numerical solutions to the inverse Cauchy problems governed by 3D elastic equations.

5.2 Test problem 2: a classical mechanical component

Next, we consider the stress analysis in a classical mechanical component, as shown in Fig. 6(a). The principal dimension of the tool is 2m in length, 1.2m in width, and 1m in height. For the numerical implementation, a total number of 1860 nodes are discretized on the whole surface of the computational domain. The SBM nodes here are created by uisng the CAE software Hypermesh, as shown in Fig. 6(b). In this example, the left-hand surface of the computational domain is under-specified where both the displacements and tractions are unknown and have to be determined.

Fig. 7 shows the relative error curves of the calculated displacements and tractions retrieved on the whole surface of the computational domain, with respect to the length

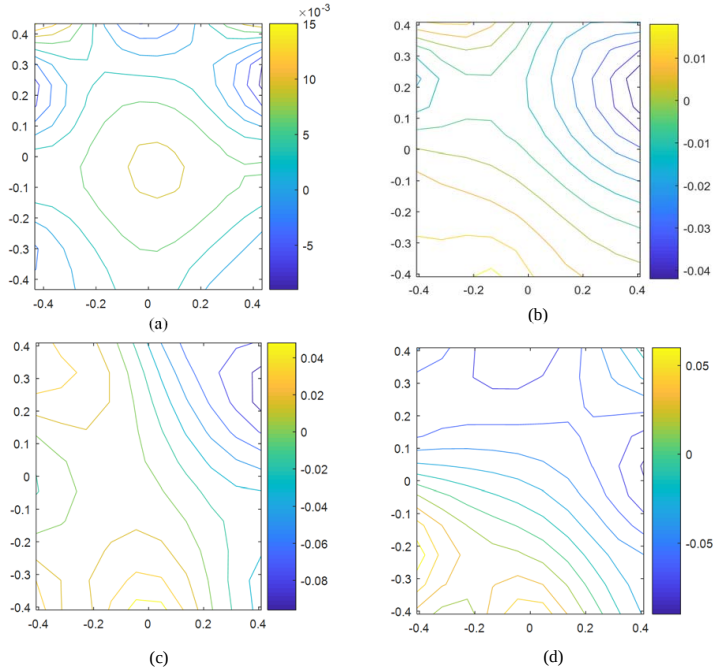

Figure 5: Error distribution for tractions t_1 retrieved on the under-specified boundary, with (a) 0% noisy, (b) 1% noisy, (c) 2% noisy, and (d) 3% noisy added into the input data.

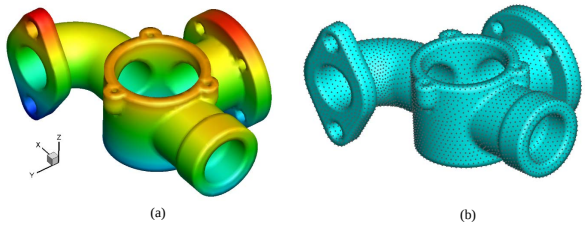

Figure 6: Geometry of the problem (a), and the configuration of the SBM nodes distribution (b).

of the accessible boundary. It can be seen from this figure that the numerical results, both for displacements and tractions, agree quite well with their corresponding analytical solutions, and as expected, the accuracy of the numerical results improves significantly as the length of the accessible boundary increases, i.e., BL increases.

Fig. 8 illustrates the L-curves for Tikhonov regularization techniques, with $BL = 0.8$ and 1% noise added into the data. The L-curve is a log-log plot of the norm of regularized solution versus the norm of the corresponding residual norm, as illustrated in Eq. (4.4). The corner point of L-curve is a compromise between the regularization errors due to data smoothing and perturbation errors in measurements or other noise. According to the L-curve criterion, the optimal value of the regularization parameter is chosen at the "corner" of the L-curve.

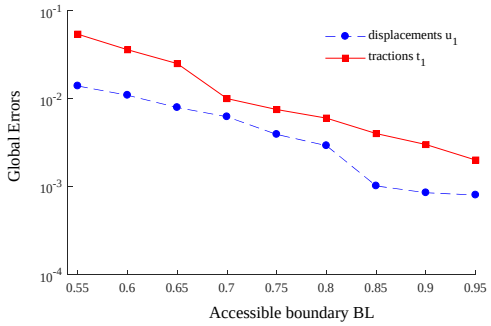

Figure 7: Relative error curves of the computed displacements and tractions with respect to the length of the accessible boundary BL.

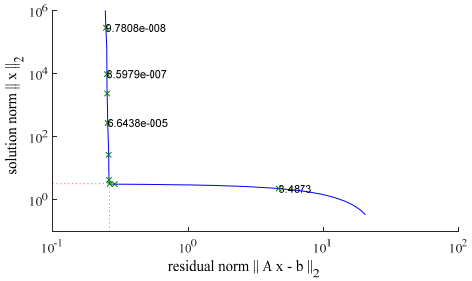

Figure 8: L-curves for Tikhonov regularization technique, with $BL=0.85$ and 1% noise added into the data.

To illustrate the convergence of the proposed method, Figs. 9(a)-(d) displays the relative error surface of displacements u_1 retrieved on the whole surface of the computational domain as functions of different number of SBM nodes. It can be seen that the present SBM is stable, accurate, and rapidly convergent as the number of nodes increases. It is also observed that the SBM results with only 826 nodes are quite accurate for this 3D case. The size of resulting system of linear algebraic equations is quite small. Although not presented here, it should be noted that analogous results have been obtained for other components of the displacement and traction vectors, as well as for displacements and stresses in the cases with other combinations of boundary conditions.

5.3 Test problem 3: inverse Cauchy in an airplane

Finally, the inverse Cauchy problem in an airplane is considered. The geometry of the problem is shown in Fig. 10 with dimension 33.2m in length, 25.5m in width, and 7.1m in height. For the numerical implementation, a total number of 26584 irregularly distributed nodes, as shown in Fig. 11, are discretized on the whole surface of the computational domain.

Figs. 12 and 13 respectively plot the exact and numerical solutions for displacements $u_1(x)$ retrieved on the whole surface of the airplane. The numerical displacements here

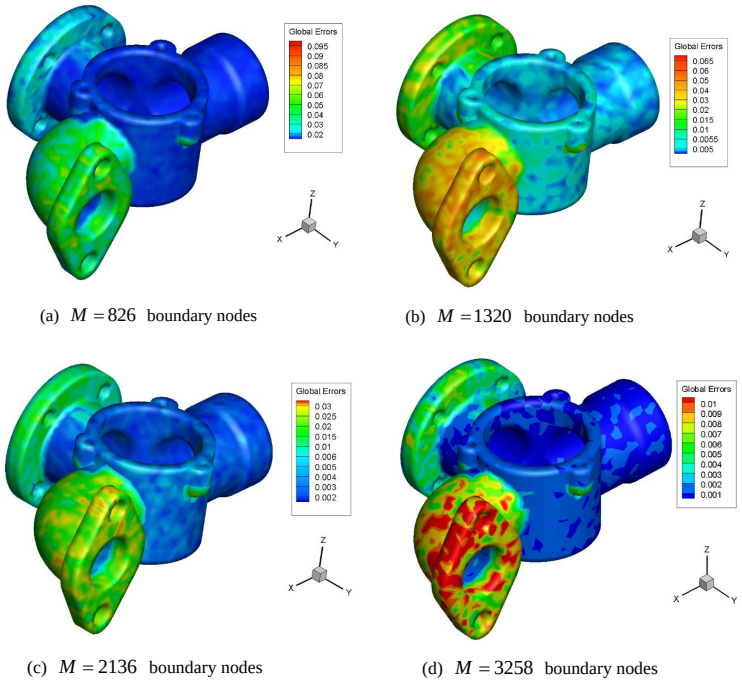

(a) $M=826$ boundary nodes (b) $M=1320$ boundary nodes

(c) $M=2136$ boundary nodes (d) $M=3258$ boundary nodes

Figure 9: The error distribution for displacements u_1 retrieved on the whole surface of the computational domain with $BL=0.7$, where the SBM nodes are 826 for (a), 1320 for (b), 2136 for (c), and 3258 for (d).

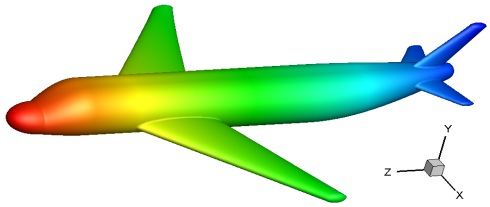

Figure 10: The sketch of an airplane.

are calculated with 2% noise added into the input data and $BL=0.7$. As can be seen from these figures, the displacement results predicted by using the proposed scheme are in quite good agreement with the analytical solution. The value of regularization parameter for this 3D model, as shown in Eq. (4.1), is $\lambda=0.026$.

Although not presented, it is reported that numerous other numerical experiments have been performed and analogous conclusions have been drawn. Overall, it can be concluded that the SBM, in conjunction with the first-order Tikhonov regularization technique and the L-curve criterion, is accurate and stable with respect to decreasing the amount of noise added into the input data and convergent with respect to increasing the number of boundary nodes. In comparison with existing methods for solving nu-

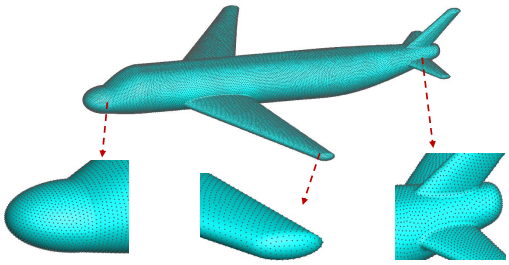

Figure 11: Configuration of the SBM nodes distribution for the airplane.

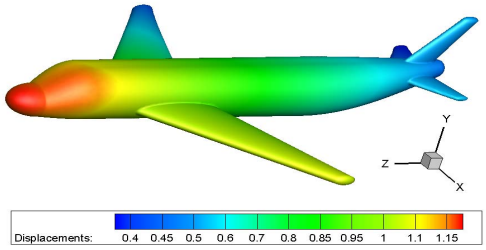

Figure 12: The analytical solution profile of the displacements u_1 on the surface of the airplane.

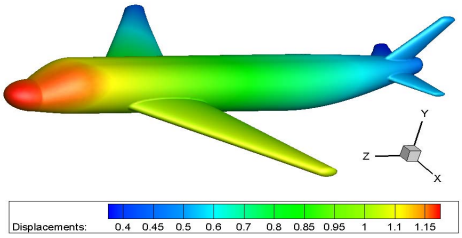

Figure 13: The numerical displacements u_1 retrieved on the whole surface of the airplane, with $BL=0.7$ and 2% noise added into the input data.

merically inverse Cauchy problems in 3D elastostatics, the proposed scheme could be considered as a competitive alternative.

6 Concluding remarks

This study documents the first attempt to apply the SBM for the efficient and accurate solutions of inverse Cauchy problems in 3D linear elasticity. The resulting ill-conditioned system of linear algebraic equations has been regularized by using the Tiknonov regularization technique, while the optimal regularization parameter was determined by the L-curve criterion. Three benchmark 3D elasticity problems clearly demonstrate the

stability and accuracy of the proposed SBM scheme. Further analyses and optimized implementation are required in order to fully explore the efficiency and accuracy of the new methods. These include the detailed convergence order analyses of the methods, optimized strategies for adaptive mesh refinements, as well as the optimal choice of many different parameters. Results along these lines will be presented in the future.

It is noted that the proposed SBM, similar to the BEM, has many inherent shortcomings compared with the powerful FEM. For example, the method cannot be used for problems whose fundamental solution is either not known or cannot be determined. The method is also not applicable to nonlinear problems for which the principle of superposition does not hold. In such case, a SBM model procedures domain integrals, which may spoil the pure boundary character of the method.

Finally, it must be pointed out that the proposed SBM to 3D elasticity problems should be considered as a complement to the FEM in the structural analysis. For structures that can be identified clearly as shells or bulky solids, the FEM should be used because of the widely available automatic meshing capabilities in the various FEM packages. For 3D structures where the solid models are difficult to obtain, the proposed schedule can be used as an alternative, especially when high accuracy is desired, as in benchmarks.

Acknowledgements

The work described in this paper was supported by the National Natural Science Foundation of China (Nos. 11402075, 11401332, 71571108), Projects of International (Regional) Cooperation and Exchanges of NSFC (No. 71611530712), the Natural Science Foundation of Shandong Province of China (Nos. ZR2017BA003, ZR2015GZ007, ZR2017JL004), the Research Grants Council of the Hong Kong Special Administrative Region (No. CityU 11204414), and the Science and Technology Innovation Commission of Shenzhen Municipality (No. JCYJ20160229165310679).

References

[1] G. R. Liu, G. Y. Zhang, Y. Y. Wang, Z. H. Zhong, G. Y. Li and X. Han, *A nodal integration technique for meshfree radial point interpolation method (NI-RPIM),* Int. J. Solids. Struct., 44 (2007), pp. 3840–3860.

[2] T. Q. Bui, A. Khosravifard, C. Zhang, M. R. Hematiyan and M. V. Golub, *Dynamic analysis of sandwich beams with functionally graded core using a truly meshfree radial point interpolation method,* Eng. Struct., 47 (2013), pp. 90–104.

[3] V. P. Nguyen, T. Rabczuk, S. Bordas and M. Duflot, *Meshless methods: A review and computer implementation aspects,* Math. Comput. Simulation, 79 (2008), pp. 763–813.

[4] J. J. Benito, F. Urena and L. Gavete, *Influence of several factors in the generalized finite difference method,* Appl. Math. Model., 25 (2001), pp. 1039–1053.

[5] Y. Gu, W. Chen, H. Gao and C. Zhang, *A meshless singular boundary method for three-dimensional elasticity problems,* Int. J. Numer. Methods. Eng., 107 (2016), pp. 109–126.

[6] A. KARAGEORGHIS, D. LESNIC AND L. MARIN, *The method of fundamental solutions for an inverse boundary value problem in static thermo-elasticity,* Comput. Struct., 135 (2014), pp. 32–39.
[7] L. MARIN, *A meshless method for solving the cauchy problem in three-dimensional elastostatics,* Comput. Math. Appl., 50 (2005), pp. 73–92.
[8] J. LI, Z. FU AND W. CHEN, *Numerical investigation on the obliquely incident water wave passing through the submerged breakwater by singular boundary method,* Comput. Math. Appl., 71 (2016), pp. 381–390.
[9] C. S. CHEN, M. GANESH, M. A. GOLBERG AND A. H. D. CHENG, *Multilevel compact radial functions based computational schemes for some elliptic problems,* Comput. Math. Appl., 43 (2002), pp. 359–378.
[10] G. FAIRWEATHER AND A. KARAGEORGHIS, *The method of fundamental solutions for elliptic boundary value problems,* Adv. Comput. Math., 9 (1998), pp. 69–95.
[11] X.-W. GAO, *A meshless BEM for isotropic heat conduction problems with heat generation and spatially varying conductivity,* Int. J. Numer. Methods. Eng., 66 (2006), pp. 1411–1431.
[12] L. MARIN AND D. LESNIC, *The method of fundamental solutions for the Cauchy problem associated with two-dimensional Helmholtz-type equations,* Comput. Struct., 83 (2005), pp. 267–278.
[13] T. BELYTSCHKO, Y. KRONGAUZ, D. ORGAN, M. FLEMING AND P. KRYSL, *Meshless methods: An overview and recent developments,* Comput. Methods. Appl. Mech. Eng., 139 (1996), pp. 3–47.
[14] D. L. YOUNG, C. C. TSAI, C. W. CHEN AND C. M. FAN, *The method of fundamental solutions and condition number analysis for inverse problems of Laplace equation,* Comput. Math. Appl., 55 (2008), pp. 1189–1200.
[15] Y. GU, W. CHEN AND X. Q. HE, *Improved singular boundary method for elasticity problems,* Comput. Struct., 135 (2014), pp. 73–82.
[16] C. YANG AND X. LI, *Meshless singular boundary methods for biharmonic problems,* Eng. Anal. Bound. Elem., 56 (2015), pp. 39–48.
[17] J. LIN, C. ZHANG, L. SUN AND J. LU, *Simulation of seismic wave scattering by embedded cavities in an elastic half-plane using the novel singular boundary method,* Adv. Appl. Math. Mech., 10 (2018), pp. 322–342.
[18] Z.-J. FU, W. CHEN AND Y. GU, *BurtonMiller-type singular boundary method for acoustic radiation and scattering,* J. Sound. Vib., 333 (2014), pp. 3776–3793.
[19] J. LIN, W. CHEN AND C. S. CHEN, *Numerical treatment of acoustic problems with boundary singularities by the singular boundary method,* J. Sound. Vib., 333 (2014), pp. 3177–3188.
[20] B. CHEN, W. CHEN, A. H. D. CHENG AND X. WEI, *The singular boundary method for two-dimensional static thermoelasticity analysis,* Comput. Math. Appl., 72 (2016), pp. 2716–2730.
[21] X. WEI, W. CHEN, B. CHEN AND L. SUN, *Singular boundary method for heat conduction problems with certain spatially varying conductivity,* Comput. Math. Appl., 69 (2015), pp. 206–222.
[22] Y. GU, X. HE, W. CHEN AND C. ZHANG, *Analysis of three-dimensional anisotropic heat conduction problems on thin domains using an advanced boundary element method,* Comput. Math. Appl., 75 (2018), pp. 33–44.
[23] Y. GU, H. GAO, W. CHEN AND C. ZHANG, *A general algorithm for evaluating nearly singular integrals in anisotropic three-dimensional boundary element analysis,* Comput. Methods. Appl. Mech. Eng., 308 (2016), pp. 483–498.
[24] B. SARLER AND R. VERTNIK, *Meshfree explicit local radial basis function collocation method for diffusion problems,* Comput. Math. Appl., 51 (2006), pp. 1269–1282.
[25] B. SARLER, *Solution of potential flow problems by the modified method of fundamental solutions:*

Formulations with the single layer and the double layer fundamental solutions, Eng. Anal. Bound. Elem., 33 (2009), pp. 1374–1382.

[26] C. S. CHEN, H. A. CHO AND M. A. GOLBERG, *Some comments on the ill-conditioning of the method of fundamental solutions,* Eng. Anal. Bound. Elem., 30 (2006), pp. 405–410.

[27] L. MARIN AND D. LESNIC, *The method of fundamental solutions for nonlinear functionally graded materials,* Int. J. Solids. Struct., 44 (2007), pp. 6878–6890.

[28] J. LIN, W. CHEN AND F. WANG, *A new investigation into regularization techniques for the method of fundamental solutions,* Math. Comput. Simul., 81 (2011), pp. 1144–1152.

[29] J. LIN, W. CHEN AND L. SUN, *Simulation of elastic wave propagation in layered materials by the method of fundamental solutions,* Eng. Anal. Bound. Elem., 57 (2015), pp. 88–95.

[30] W. CHEN AND F. Z. WANG, *A method of fundamental solutions without fictitious boundary,* Eng. Anal. Bound. Elem., 34 (2010), pp. 530–532.

[31] W. QU AND W. CHEN, *Solution of two-dimensional stokes flow problems using improved singular boundary method,* Adv. Appl. Math. Mech., 7 (2015), pp. 13–30.

[32] F. WANG, W. CHEN, C. ZHANG AND J. LIN, *Analytical evaluation of the origin intensity factor of time-dependent diffusion fundamental solution for a matrix-free singular boundary method formulation,* Appl. Math. Modell., 49 (2017), pp. 647–662.

[33] X. WEI, B. CHEN, S. CHEN AND S. YIN, *An ACA-SBM for some 2D steady-state heat conduction problems,* Eng. Anal. Bound. Elem., 71 (2016), pp. 101–111.

[34] Y. GU, W. CHEN, C. ZHANG AND X. HE, *A meshless singular boundary method for three-dimensional inverse heat conduction problems in general anisotropic media,* Int. J. Heat. Mass. Transf., 84 (2015), pp. 91–102.

[35] Y. GU, W. CHEN AND B. ZHANG, *Stress analysis for two-dimensional thin structural problems using the meshless singular boundary method,* Eng. Anal. Bound. Elem., 59 (2015), pp. 1–7.

[36] Y. GU, H. GAO, W. CHEN, C. LIU, C. ZHANG AND X. HE, *Fast-multipole accelerated singular boundary method for large-scale three-dimensional potential problems,* Int. J. Heat. Mass. Transf., 90 (2015), pp. 291–301.

[37] C. M. FAN, Y. K. HUANG, P. W. LI AND C. L. CHIU, *Application of the generlized finite-difference method to inverse biharmonic boundary-value problems,* Numerical Heat Transfer Part B-Fundamentals, 65 (2014), pp. 129–154.

[38] A. KARAGEORGHIS, D. LESNIC AND L. MARIN, *A survey of applications of the MFS to inverse problems,* Inverse. Probl. Sci. Eng., 19 (2011), pp. 309–336.

[39] L. MARIN, *Boundary elementminimal error method for the Cauchy problem associated with Helmholtz-type equations,* Comput. Mech., 44 (2009), pp. 205–219.

[40] L. MARIN, *A meshless method for the stable solution of singular inverse problems for two-dimensional Helmholtz-type equations,* Eng. Anal. Bound. Elem., 34 (2010), pp. 274–288.

[41] P. C. HANSEN AND D. P. O'LEARY, *The use of the L-curve in the regularization of discrete ill-posed problems,* SIAM J. Sci. Comput., 14 (1993), pp. 1487–1503.

[42] A. POULLIKKAS, A. KARAGEORGHIS AND G. GEORGIOU, *The method of fundamental solutions for three-dimensional elastostatics problems,* Comput. Struct., 80 (2002), pp. 365–370.

[43] Y. GU, W. CHEN AND C.-Z. ZHANG, *Singular boundary method for solving plane strain elastostatic problems,* Int. J. Solids. Struct., 48 (2011), pp. 2549–2556.

[44] M. GUIGGIANI AND P. CASALINI, *Direct computation of Cauchy principal value integrals in advanced boundary elements,* Int. J. Numer. Methods. Eng., 24 (1987), pp. 1711–1720.

[45] D. E. BESKOS, *Boundary element methods in dynamic analysis,* Appl. Mech. Rev., 40 (1987), pp. 1–23.

[46] D. E. BESKOS, *Boundary element methods in dynamic analysis: part II (1986-1996),* Appl. Mech.

Rev., 50 (1997), pp. 149–197.

[47] Y. GU, W. CHEN AND Z.-J. FU, *Singular boundary method for inverse heat conduction problems in general anisotropic media,* Inverse. Probl. Sci. Eng., 22 (2013), pp. 889–909.